JOURNAL OF MECHANICAL ENGINEERING, SCIENCE, AND INNOVATION
ITATS
Research Article

Optimizing Effect of Wavy Leading Edge (WLE) in Rectangular Wing and Taper Wing

Journal of Mechanical Engineering, Science, and Innovation
e-ISNN: 2776-3536
2021, Vol. 1, No. 2
DOI: 10.31284/j.jmesi.2021.v1i2.2296
ejurnal.itats.ac.id/jmesi

Iis Rohmawati[1], Hiroshi Arai[2], Hidemi Mutsuda[1], Takuji Nakashima[1], Rizal Mahmud[3]

[1]Hiroshima University, Japan
[2]Japan Marine United Corporation, Japan
[3]Institut Teknologi Adhi Tama Surabaya, Indonesia

Corresponding author:
Iis Rohmawati
Hiroshima University, Japan
Email: d161420@hiroshima-u.ac.jp

Abstract

Experimental and numerical research have been performed to investigate the Wavy Leading Edge (WLE) effect on the rectangular wing. The WLE is inspired by humpback whale flipper morphology which is blunt and rounded in certain form pattern. This flipper shape plays an important role for its behaviour specially capturing their prey. This advantage could be applied to other systems such as fin stabilizers or wind turbines. Steady cases in various aspect ratios were conducted to find out the optimum effect of WLE with baseline NACA 0018 profile at Reynolds number 1.4 x 10^5. The chord length of the wing (c) was 125 mm. The WLE shape defined as wavelength (W) 8% of c and amplitude (d) is 5% of c. The aspect ratio (AR) variations were 1.6; 3.9; 5.1; 7.9 and 9.6. A simple rectangular form of the wing was selected to analysis the WLE effect on the various ARs. The taper wing shape is applied to find out the WLE effect at the AR 7.9. three types of taper ratio (TR) are 0.1; 0.3 and 0.5. The results show that the WLE on the taper wing has better advantage to control the stall in steady case. Another impressive result was the WLE wing with AR 7.9 and TR 0.3 has the best lift coefficient and pressure distribution.

Keywords: *Stall, wavy leading edge, steady case, rectangle wing, taper wing, aspect ratio.*

Date received: October 14, 2021; accepted: October 29, 2021

Handling Editor: Indah Puspitasari

INTRODUCTION

Inspired by humpback whale flipper which has unique shape around its leading edge. It has capability to catch their prey with blunt and round form in the leading edge. It was described in Figure 1. Pioneer research has been done by Fish, et. al. [1] explored the morphology of humpback whale flipper. Its flipper had typical design to improve hydrodynamic performance. The tubercle on the leading edge of its flipper has an important role to increase the lift and delaying stall [2]. Talking about application of bio-inspired technology, the tubercle has a potential function in the design control of fluid flow such as on the fin stabilizer and wind turbines [3].

Figure 1. Humpback Whale with tubercles on flipper leading edge (http://oceanwideimages.com)

Experimental research using a scallop flipper were employed by Miklosovic et. al. [4], [5]. The scallop flipper has an impressive performance to delay stall and increase the lift force after stall condition. The flow behavior and lift forces generation on tubercles wing has been explored by Hansen et. al., [6], [7], [8]. Most effective tubercles were found for smallest amplitude and wavelength that able to acquire the higher lift coefficient. Counter-rotating vortex was found in the tubercles. Arai et. al. [9], [10] conducted experimental and numerical research to find out the mechanism of stall delay on the wavy leading edge (WLE) wing. They found that the WLE wing can restrain flow separation and delay stall.

Another experimental research was done by Huang et. al. [11] that explored effect of protuberances leading edge on the Horizontal Axis Wind Turbines (HAWT). The protuberances leading edge were effectively delay the stall. Lin et. al. [12] performed research with wavy leading edge and wavy trailing edge wing on the VAWT. They applied the SST k-ω turbulence model in their numerical research. The wavy leading edge has capability to increase the thrust force than the wavy trailing edge. Wang et. al. [13] conducted a research using serration of leading edge on the VAWT with rotating motion. The flow separation was significantly suppressed due to existence of serration on the leading edge. Shi et. al. explored the undulated leading edge on tidal turbines. Their result was the undulated leading edge has a stable hydrodynamic performance for varied current speed and waves.

Javaid et. al. [14] performed the experimental and numerical work for underwater glider application between rectangular and tapered wing. Even though the taper wing has lower lift force, it could improve the dynamic stability. Similar research has been done by Wei et. al. [15] using tubercles on tapered swept back wing for underwater glider application. The tubercles wing leads to a longer cruise range. Our recent research obtained an experimental of wavy leading edge which is applied to the rectangular and taper wing. The taper wing with WLE able to acquire the lift coefficient after stall condition. The WLE has suppression effect on taper wing.

The WLE is not the only one device to control the fluid flow on the wing. Other devices that used to control the stall are Vortex Generator (VG), Elevated Wire (EW) and cavity [16]. The cavity acted as a reservoir of flow and no beneficial effect after stall

condition. The VG and EW able to improve the post-stall characteristics of the wing. But the VG is inefficient to improve the lift forces after stall condition. VG able to suppress the stall below angle of attack 20° [17]. Due to the effectiveness to control the stall, the WLE was applied in this research.

The above studies were mentioned have clarified that the WLE on the wing has favorable lift coefficient after stall condition. This is a potential benefit to apply in practical application such as fin stabilizer and wind turbine. There is no research observing the optimum aspect ratio on the WLE wing. Beside that the WLE effect on the wing shape should be explored to find out the maximum advantages by using WLE application. In this study, two types of wing shape were given as comparison.

METHODS

Experimental Method

A NACA 0018 profile was chosen as baseline wing in this study. The experimental study has been conducted by using circular water channel in Hiroshima University, Japan. In the first section, the wing scheme and WLE shape was described. The origin coordinate system (*O-xyz*) was located on the leading edge where *x*-axis is parallel to the flow direction, *y*-axis is parallel to the span direction of the wing as described in Figure 2. This study was performed with four AR i.e. 1.6; 3.9; 5.1; 7.9 and 9.6. The chord length (*c*) of the wing is 125 mm. The WLEs were placed in the leading edge of the wing with wavelength (*W*) is 8% of *c* and amplitude (*d*) is 5% of *c*. Figure 3 shows the schematic view of WLE wing. The shape of WLE is determined as follows:

$$x_{WLE\,(y)} = x_{LE} - \left[\frac{d}{2}\sin\left\{\frac{2\pi}{W}\left(y - \frac{W}{4}\right)\right\} + \frac{d}{2}\right] \qquad (1)$$

, where x_{LE} is *x*-coordinate of baseline wing, x_{WLE} is *x*-coordinate for WLE, *W* and *d* is wavelength and amplitude of WLE, respectively. Plane view of the wings were described in Figure 4 with baseline and WLE wing. Symmetry plane in the plane view was denoted as “SP”.

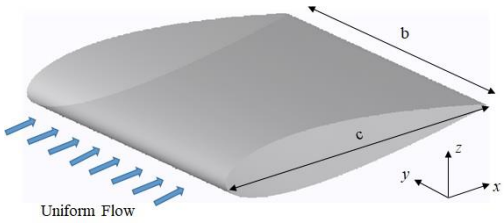

Figure 2. Coordinate system

To approach the humpback whale flipper shape, this study not only employed in rectangular wing only, but also using taper wing with three types of Taper Ratio (TR). The TR types was 0.1; 0.3, and 0.5 with AR 7.9 as described in Figure 5. The TR was defined as follows:

$$\text{TR} = \frac{c_{wing\ tip}}{c_{root}} \qquad (2)$$

where, $c_{\text{wing tip}}$ is wing tip chord length (m) with c_{root} is root chord length (m). Meanwhile the average chord ($\bar{c}$) of taper wing is similar with the chord length of rectangular wing i.e. 125 mm.

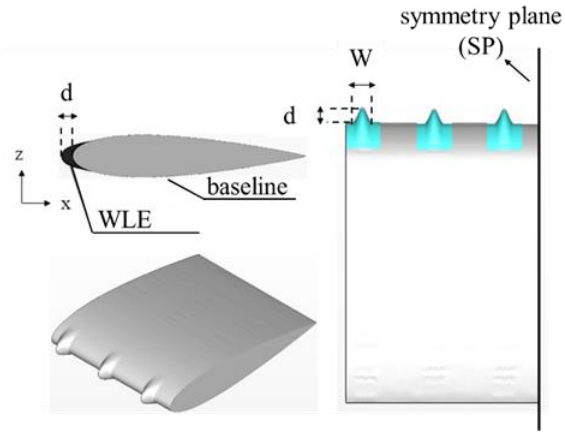

Figure 3. Schematic view of WLE

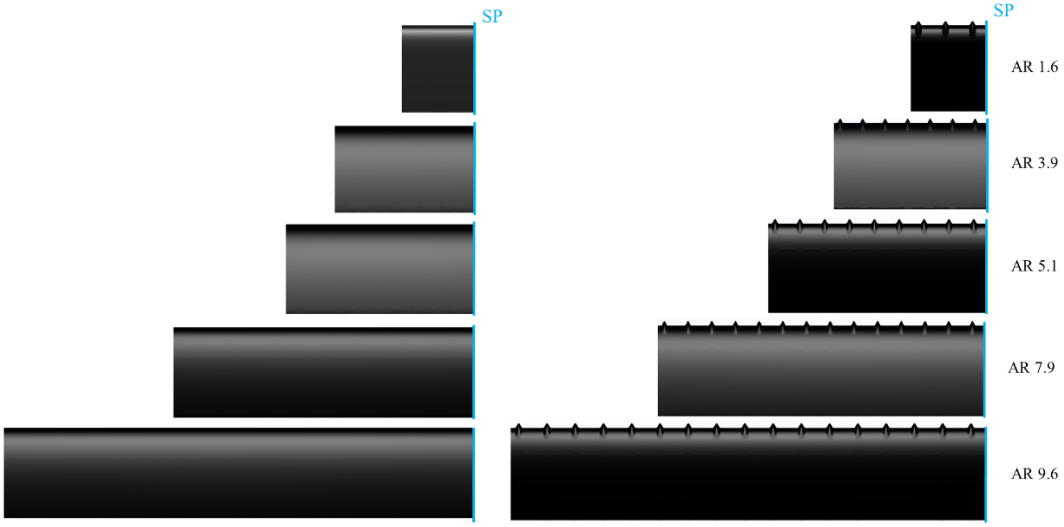

(a) Baseline wing (b) WLE wing

Figure 4. Plane view of the wings

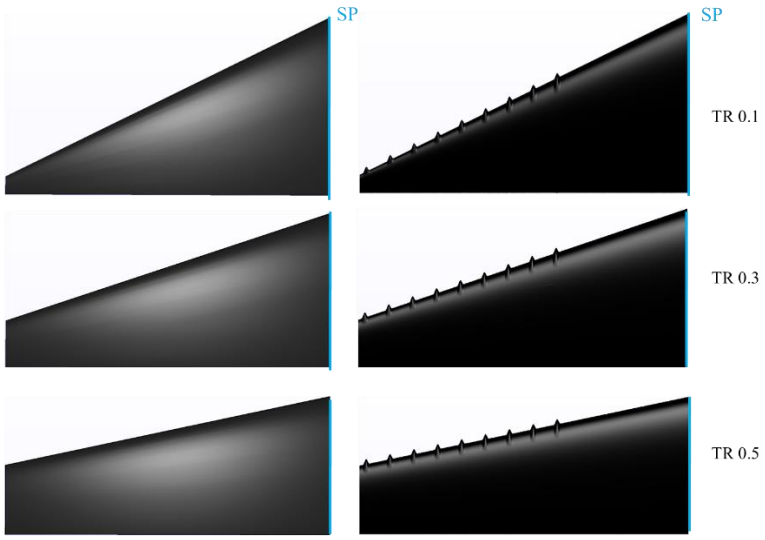

Figure 5. Plane view of taper wing in various TR

Measuring cross section of circular water channel has a width 1.4 m, height 1.0 m and length 3.3 m. Figure 6 shows the experimental set-up of the wing during steady case. The circular water channel has the depth 0.9 m where the wing is placed 0.9 m from

inlet flow and 0.15 m from the upper surface. Due to the limitation of circular water channel, the experimental study only performed at AR 1.6; 3.9 and 5.1 only. The blockage ratio was adjusted to keep the distance between wing tip and the bottom surface of circular water channel. Blockage ratio 8% was applied in this study where the blockage ratio is defined as follows:

$$\text{Blockage ratio} = \frac{AR\ c^2}{d} \qquad (3)$$

where, AR is aspect ratio of the wing, c is chord length (m), and d is depth of outer boundary (m).

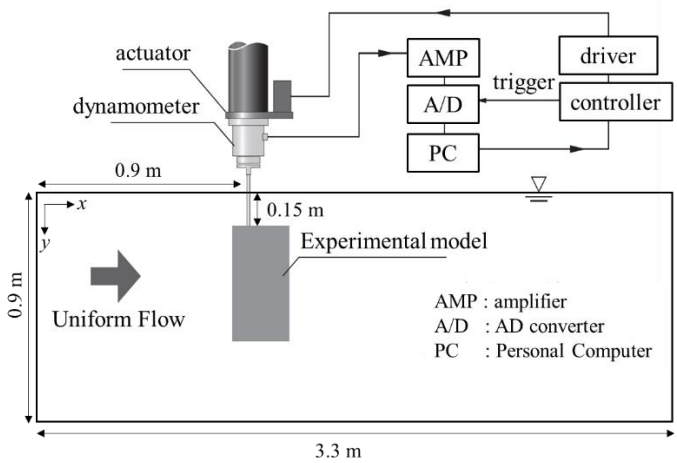

Figure 6. Experimental set-up

Numerical Method

Numerical studies were carried out by using Computational Fluid Dynamics (CFD) with turbulence model SST k-ω. This turbulence model is capable to capture the forces and flow structures well with the experimental data [20], [21], [22], [23], [24], [25]. By using CFD, the forces and flow pattern distribution on the wing were capable to be explored. The lift coefficient (C_L) and the drag coefficient (C_D) defined as follows:

$$C_L = \frac{L}{\frac{1}{2}\rho |U_0|^2 s\, c} \qquad (4) \qquad C_D = \frac{D}{\frac{1}{2}\rho |U_0|^2 s\, c} \qquad (5)$$

where, L : lift force, D : drag force, s : span, c : chord length, ρ : fluid density, U_0 : free-stream velocity (m/s).

The unstructured trapezoidal meshing was chosen in this simulation where 10 layers were applied around the wing. Figures 7-8 show the mesh configuration on both wings. Figure 9 describes the domain simulation of AR 3.9 during steady case. The outer boundary for higher AR were adjusted to catch the similar blockage ratio. The chord length of the wing was c where it placed 7.2 times of c from the inlet. The inlet boundary condition was set to uniform velocity, the outer boundary condition was pressure, then others were set as symmetry. In this case, the half span of the wing was applied.

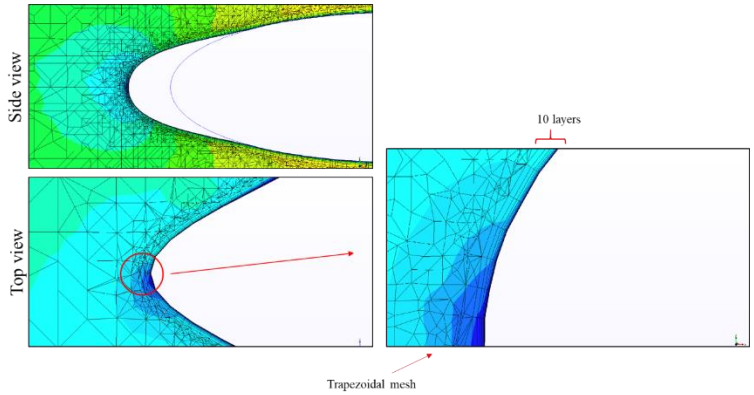

Figure 7. Layer thickness around leading edge

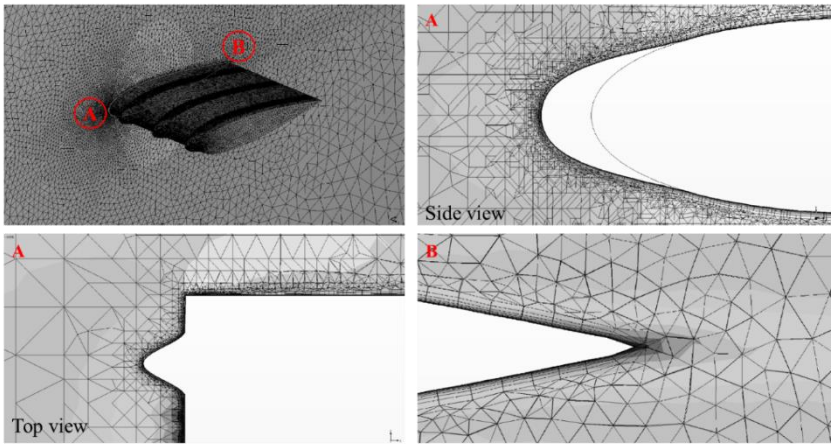

Figure 8. Meshing configuration for WLE wing

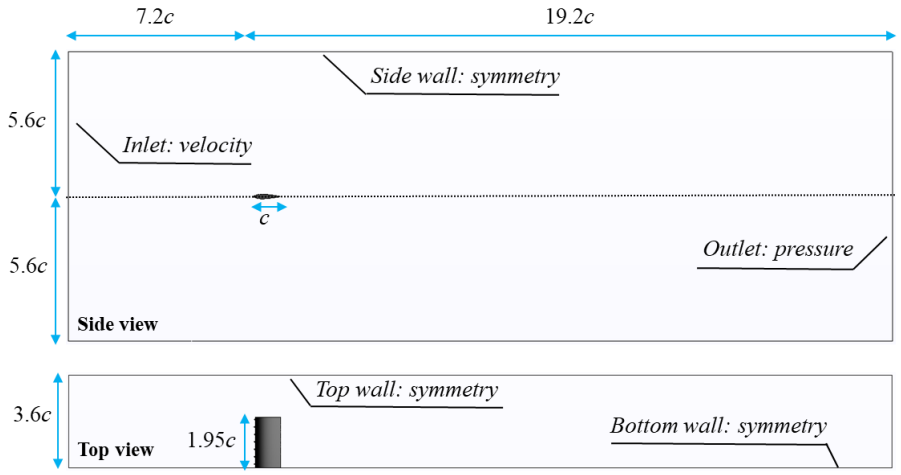

Figure 9. Domain simulations and its boundary condition (AR 3.9)

RESULTS

Rectangular wing

Grid independency study should be required to establish the accuracy of the numerical analysis. The AR 1.6 was chosen for the grid independency study at angle of attack α = 25°. This angle of attack was in the post stall regime where the WLE has superior lift coefficient. In this case, three types of mesh configuration have been applied as shown in the Table 1. The number of elements is shown in each type of mesh. Each type of the mesh configuration was compared to the experimental data then calculate

the deviation. Ratio L/D was used to analysis the convergencies. Personal computer with 128 GB of RAM was employed to this numerical simulation where time consuming was one million elements per hour. Based on the deviation, medium mesh configuration has the lowest deviation 3.43%. Next, the medium mesh configuration was employed in the following simulations.

Table 1. Grid convergence

	Total Elements of Mesh	L/D	% deviation
Experimental	-	2.08	-
Coarse	3,160,847	2.00	3.91
Medium	11,407,996	2.01	3.43
Fine	20,838,293	1.81	12.85

In the following figures are the lift coefficient (*Cl*) and drag coefficient (*Cd*) in certain angle at AR 1.6. Figures 10-11 are comparison of experimental and numerical results for lift coefficient (*Cl*) and drag coefficient (*Cd*), respectively. In general, the tendencies of numerical results were quite good compared to the experiments. As expected, the WLE wing able to acquire the lift coefficient (*Cl*) after stall condition at angles α > 18°. WLE wing has superior forces after post-stall region compared to the baseline wing [18]. To analyze the WLE effect in various AR, L/D ratio has been carried out after stall condition i.e. at angles 20°, 25°, and 30° as described in Figure 12.

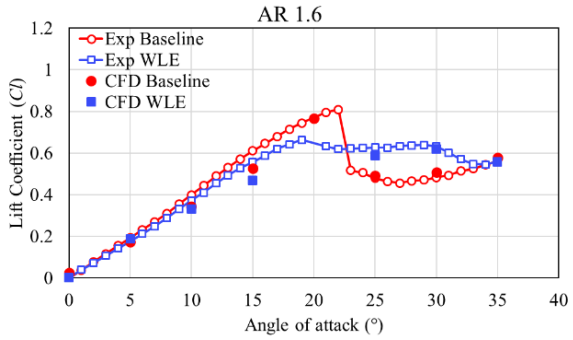

Figure 10. Lift coefficient (*Cl*) at AR 1.6

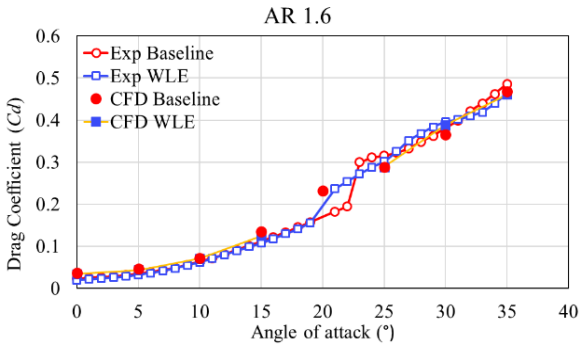

Figure 11. Drag coefficient (*Cd*) at AR 1.6

In Figure 12 shows the lift coefficient (*Cl*) and drag coefficient (*Cd*) of both wings in various AR. In this section, we are focused on the post stall region only at angles 20°, 25°, and 30°. The effectiveness of AR is necessary to be explored to find out the optimum AR. Regarding the results in the Figure 12, drag coefficient (*Cd*) has similar tendency for baseline and WLE wing. Meanwhile, the lift coefficient (*Cl*) has slightly differences. Increasing the AR could posses a higher lift coefficient (*Cl*) as mentioned in previous research [19]. The optimizing AR is necessary to be explored to get the benefit of WLE effect for some utilities such as fin stabilizer and wind turbine. Based on the results in the Figure 12, AR 7.9 has the highest lift coefficient (*Cl*) at angle of attack 20°, 25°, and 30° on WLE wing. We may conclude that WLE wing at AR 7.9 is the best performance. To get a better understanding, the flow pattern on the wing was discussed in the next section.

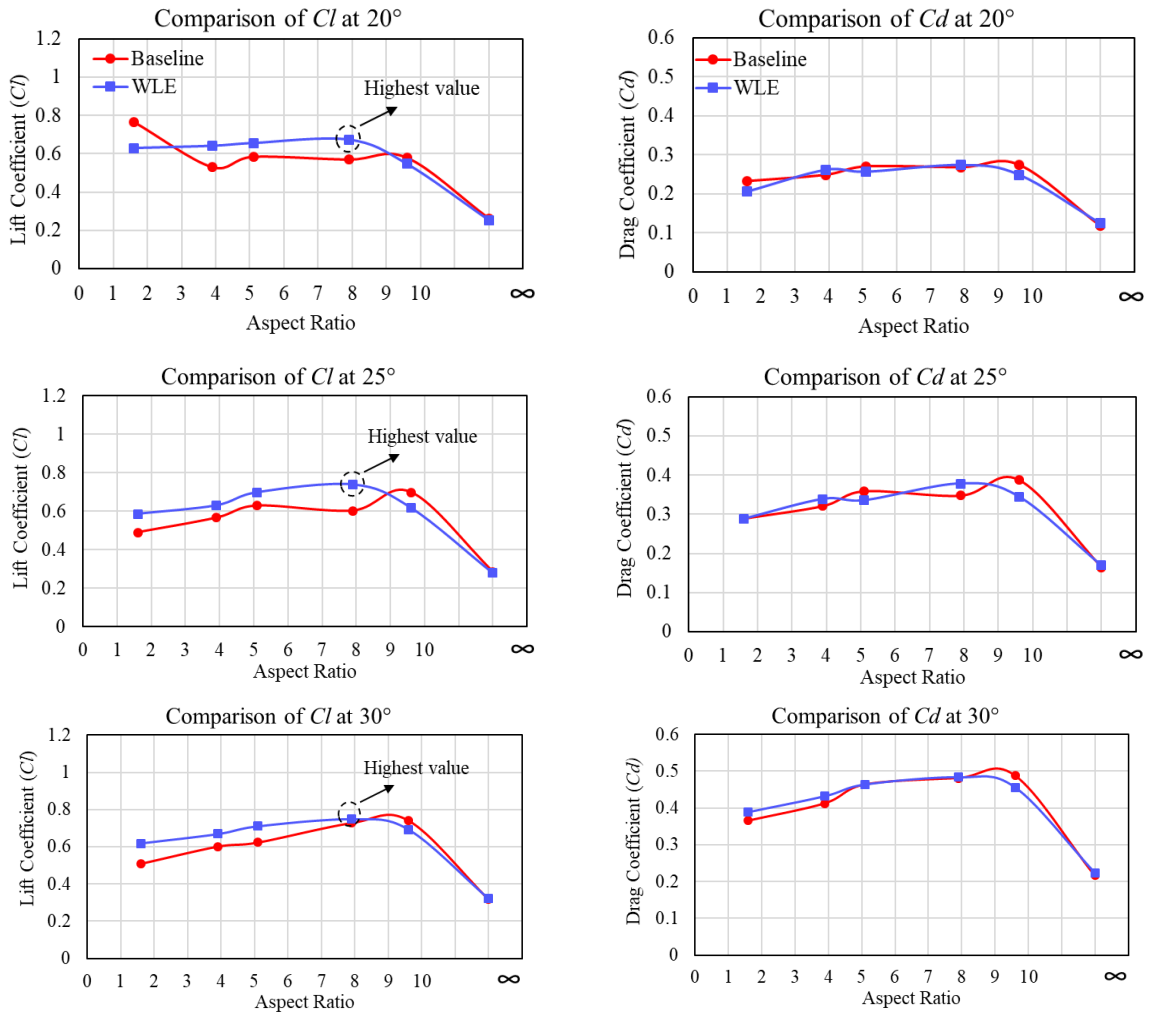

Figure 12. L/D ratio at angles 20°, 25°, and 30° in various AR

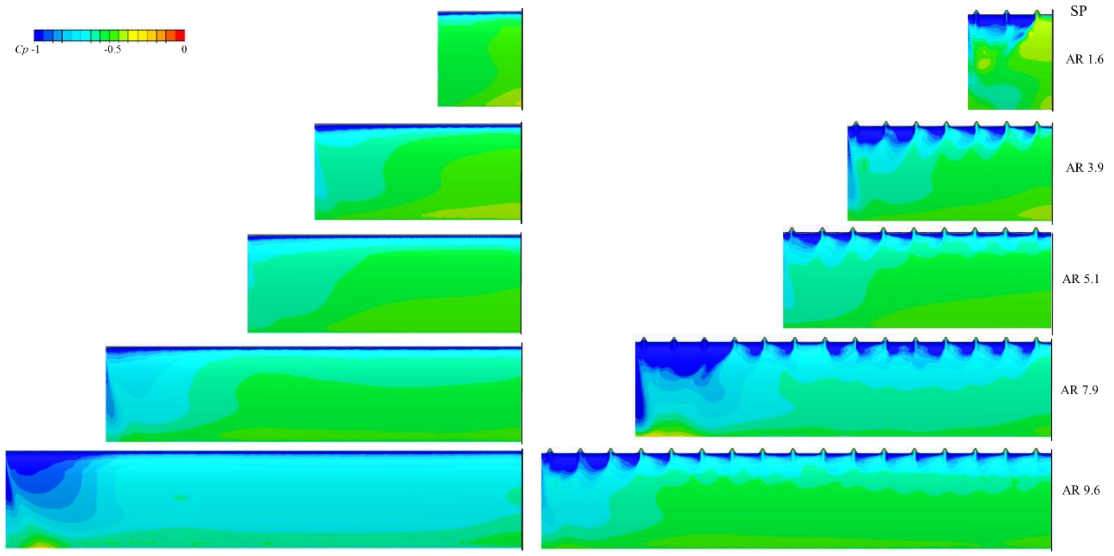

a) Baseline wing b) WLE wing

Figure 13. Pressure coefficient (*Cp*) on the upper surface of the wing at angle α = 25°

Figure 13 describes the pressure coefficient (*Cp*) distribution on the upper surface of the wing in various AR. The lower *Cp* has been found around the leading edge as shown as the blue region area. This lower *Cp* indicates that the fluid flow through easier on the surfaces than other side. Significant differences of lower *Cp* were found between baseline and WLE wing. The lower *Cp* in the leading edge was wider on the WLE wing compared to the baseline wing in various AR. In other hand, the WLEs existence could control the separation flow on the wing. This interested phenomena could improve the performance of the wing. Foremost differences blue region area was found on the WLE wing at AR 7.9 specially around the wing tip area. This hypothesis was agreed with the lift coefficient (*Cl*) comparison as mentioned in Figure 12. The optimizing of AR on the WLE wing is at AR 7.9 where the flow separation has been controlled due to the WLEs existence. The humpback whale flipper aspect ratio varies from 3.6 to 7.7 [26]. Further investigation of the wing by using WLE is still needed to improve its performance. The next section will be investigated how important the WLE on the modified wing shape into taper wing.

Taper wing

In this section, a comparison of wing shape will be discussed to find out the maximum benefit of WLE on the wing. As mentioned before, 7.9 on rectangular wing is the optimum AR with highest lift coefficient (*Cl*) after stall condition. This AR is similar to the AR range of humpback whale flipper i.e. 7.7. To improve the wing performance, the wing shape has been modified into taper wing shape with three types of Taper Ratio (TR). The WLE shape in taper ratio was similar to rectangular wing.

Validation for numerical work of taper wing has been accomplished by comparison with experimental data. The root chord length and tip chord length were 200 mm and 57 mm, respectively. Aspect ratio (AR) was 7.74. Figure 14 shows the comparison of experimental and numerical works of the validation. The mesh set-up in this numerical study was following the rectangular wing as discussed above. The tendencies of numerical result were quite agreed with the experimental result. Further work has been employed with numerical research only for taper wing with three types of TR.

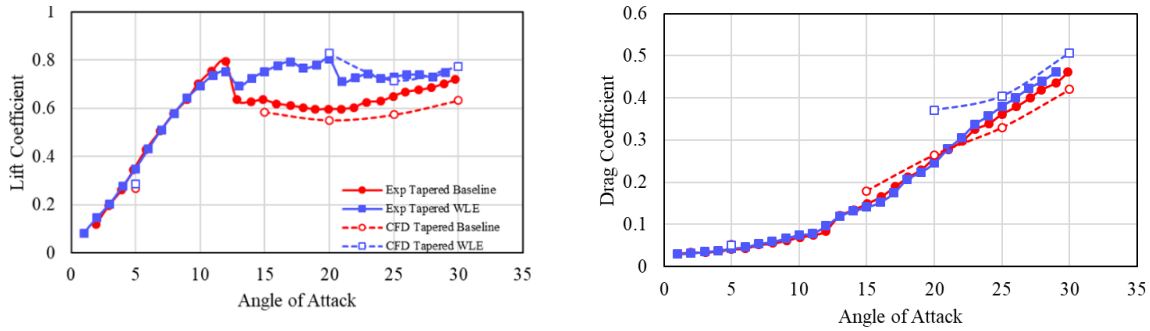

a) Lift coefficient of taper wing b) Drag coefficient of taper wing

Figure 14. Comparison of *Cl* and *Cd* on taper wing

Similar to the rectangular wing, the analysis of taper wing only focused on the angle of attack after stall condition, i.e. 20°, 25°, and 30°. Figure 15 describes the lift coefficient (*Cl*) in various TR. As expected, the WLE wing with 0.3 TR has highest value

in three angles of attack. Then, this type of taper wing will be compared to the rectangular wing to find out the best performance regarding the wing shape.

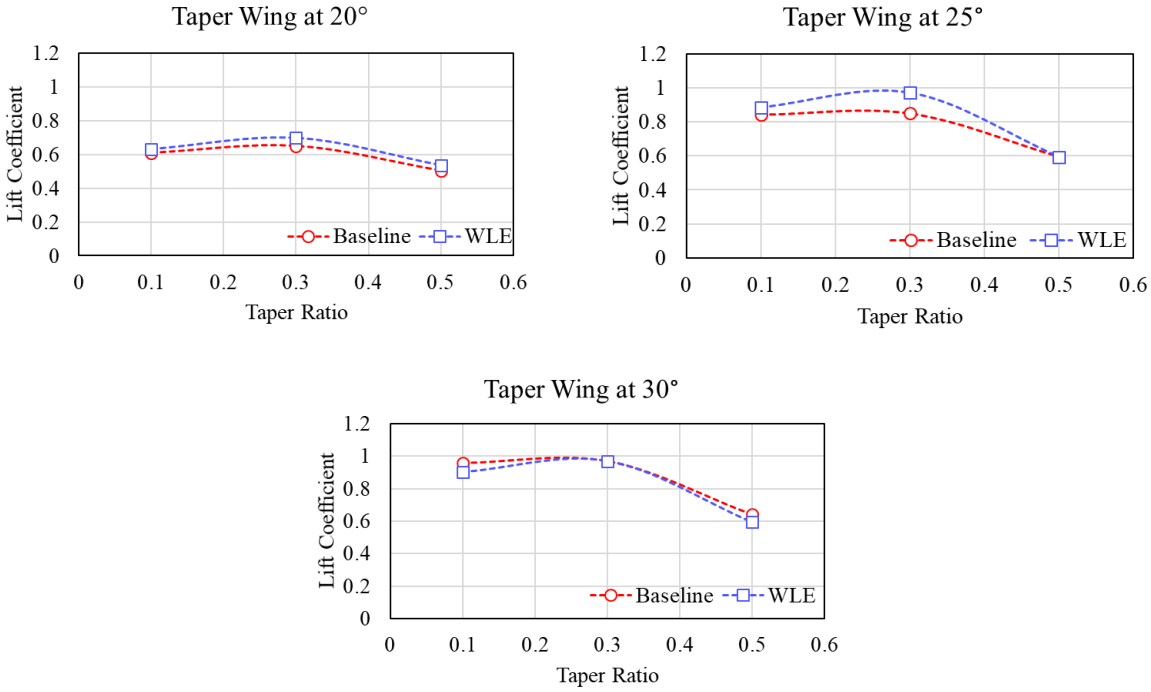

Figure 15. Lift coefficient (*Cl*) of taper wing

To clarify the WLE effect in both wing shape, the WLE location was evaluated in pressure coefficient (*Cp*) distribution as shown in Figures 17. This comparison evaluated at angle of attack 20° only. The pressure coefficient (*Cp*) distribution showed in *x-y* plane direction with 4 points located around the WLEs. The plane section is illustrated in Figure 16 with numbering system started from the wing tip. In general, lower pressure coefficient (*Cp*) distribution shown as blue region around the leading edge. Decreasing the pressure coefficient means that the flow is easier to through the wing. As shown in Figure 17, wider area of lower *Cp* distribution was found on the taper wing TR 0.3 in four sections plane. On the other hand, stronger effect of WLE was significant on taper wing. It made the taper wing unable to improve the performance.

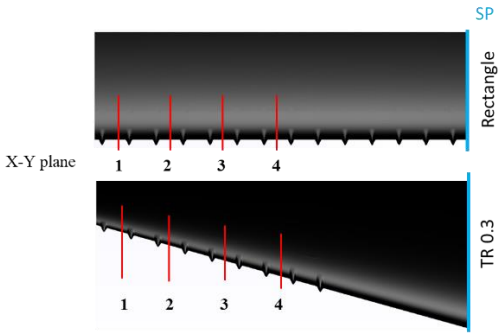

Figure 16. Numbering system of *XY*-plane

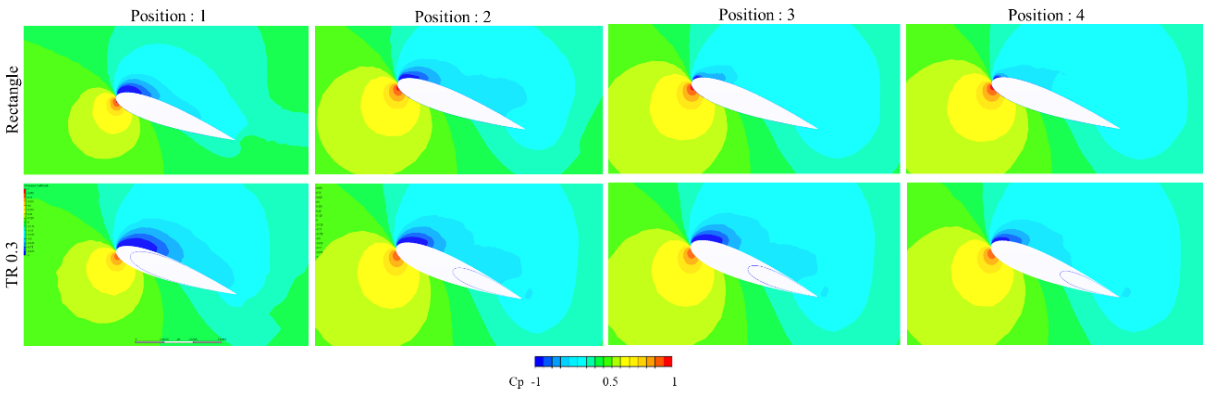

Figure 17. Pressure coefficient (*Cp*) distribution at 20°

As discussed above that the WLE shape was inspired by humpback whale flipper. In this study, two types of wing shape have been obtained to clarify the WLE effect. A simple approaching to the flipper shaper, the rectangular wing shape is chosen to explore the optimum of aspect ratio (AR) of the wing. Then the wing shape is modified into taper shape. Prove that the existence of WLE on the wing brings a potential feature to improve the wing performance. Further research should be obtained not only during steady case but also in unsteady case. This could make the maximum benefit of WLE which is used in application such as fin stabilizer, wind turbines, and helicopter blade.

CONCLUSION

The effect of Wavy Leading Edge (WLE) on NACA 0018 profile has been evaluated in experimental and numerical research during steady case. The conclusion obtained is clarified as follows:

- Inspired by humpback whale flipper which has the flipper with tubercles on their flipper, the WLE wing research has been done on rectangular wing. Optimizing the aspect ratio is needed to get the maximum benefit of tubercles. Five aspect ratios were applied in this study. Aspect ratio 7.9 has the best performance after stall condition.
- The WLE wing has favorable benefit to generate the lift force after stall condition. The lift force unable to acquire after stall condition. Furthermore, the stall point has been delayed.
- Aspect Ratio (AR) 7.9 has the optimum lift coefficient on rectangular wing. This AR is close to the AR range of humpback whale flipper.
- Optimum AR on rectangular wing has been modified into taper wing shape with three types of Taper Ratio (TR). The modified wing shape has been obtained to clarify the WLE effect on the wing. The wing with AR 7.9 and taper ratio (TR) 0.3 is the best configuration on the WLE wing.

ACKNOWLEDGMENT

The experimental works has been done in circular water channel at Hiroshima University, Japan. Thankfully to Prof. Yasuaki Doi as a former supervisor and all member of Fluid Dynamic for Vehicles Laboratory in Transportation and Environmental Systems Department, Hiroshima University, Japan.

DECLARATION OF CONFLICTING INTERESTS

The author(s) declared no potential conflicts of interest with respect to the research, authorship, and/or publication of this article.

FUNDING
The author(s) disclosed receipt of the following no financial support for the research, authorship, and/or publication of this article.

REFERENCE

[1] J. M. B. Frank E. Fish, "Hydrodynamics Design of The Humpback Whale Flipper." *Journal of Morphology* 225 : 51 - 60 (1995), pp. 51–60, 1995.
[2] F. E. Fish, P. W. Weber, M. M. Murray, and L. E. Howle, "The Tubercles on Humpback Whales ' Flippers : *Application of Bio-Inspired Technology*," vol. 51, no. 1, pp. 203–213, 2011.
[3] F. E. Fish, "Biomimetics : Determining engineering opportunities from nature," *Proc. SPIE*, vol. 7401, pp. 1–11, 2009.
[4] D. S. Miklosovic and M. M. Murray, "Experimental Evaluation of Sinusoidal Leading Edges," *Journal of Aircraft.*, vol. 44, no. 4, pp. 2–5, 2007.
[5] D. S. Miklosovic, M. M. Murray, L. E. Howle, and F. E. Fish, "Leading Edge Tubercles Delay Stall on Humpback Whale (Megaptera Novaeangliae) Flippers," *Phys. Fluids*, vol. 16, no. 5, pp. 39–42, 2004.
[6] K. L. Hansen,. N. Rostamzadeh, R. M. Keslo, B. B. Dally, "The Effect of Wavy Leading Edge Modifications on NACA 0021 Airfoil Characteristics," *18th Aust. Fluid Mechanic Conference*, no. December, 2012.
[7] K. L. Hansen, R. M. Kelso, and B. B. Dally, "Performance Variations of Leading-Edge Tubercles for Distinct Airfoil Pro fi les," *AIAA Journal*, vol. 49, pp. 185–194, 2011.
[8] K. L. Hansen, N. Rostamzadeh, and R. M. Kelso, "Evolution of the streamwise vortices generated between leading edge tubercles," *Journal of Fluid Mechanic*, vol. 788, pp. 730–766, 2016.
[9] H. Arai, Y. Doi, T. Nakashima, and H. Mutsuda, "Hydrodynamic Performance of Wing with Wavy Leading Edge," *Adv. Marit. Eng. Conf. 4th Pan Asian Assoc. Marit. Eng. Soc. Forum*, no. 2009, pp. 978–981, 2010.
[10] H. Arai, Y. Doi, T. Nakashima, and H. Mutsuda, "A Study on Stall Delay by Various Wavy Leading Edges," *Journal Aero Aqua Bio-mechanisms*, vol. 1, no. 1, pp. 18–23, 2010.
[11] G. Huang, Y. C. Shiah, C. Bai, and W. T. Chong, "Experimental study of the protuberance effect on the blade performance of a small horizontal axis wind turbine," *J. Wind Eng. Ind. Aerodyn.*, vol. 147, pp. 202–211, 2015.
[12] S. Lin, Y. Lin, C. Bai, and W. Wang, "Performance analysis of vertical axis wind turbine blade with modified trailing edge through computational fl uid dynamics," *Renewable Energy*, vol. 99, pp. 654–662, 2016.
[13] Z. Wang, Y. Wang, and M. Zhuang, "Improvement of the aerodynamic performance of vertical axis wind turbines with leading-edge serrations and helical blades using CFD and Taguchi method," *Energy Convers. Manag.*, vol. 177, no. September, pp. 107–121, 2018.
[14] M. Y. Javaid, M. Ovinis, F. B. M. Hashim, A. Maimun, Y. M. Ahmed, and B. Ullah, "Effect of wing form on the hydrodynamic characteristics and dynamic stability of an underwater glider," *Int. J. Nav. Archit. Ocean Eng.*, vol. 9, no. 4, pp. 382–389, 2017.
[15] Z. Wei, T. H. New, L. Lian, and Y. Zhang, "Leading-edge tubercles delay fl ow separation for a tapered swept-back wing at very low Reynolds number," *Ocean Eng.*, vol. 181, no. April, pp. 173–184, 2019.
[16] R. K. A. Choudry, M. Arjomandi, "Lift Curve Breakdown for Airfoil undergoing Dynamic Stall," *19th Australas. Fluid Mech. Conf.*, no. December, 2014.

[17] C. Bak, P. Fuglsang, J. Johansen and I. Antoniou, *Wind Tunnel Tests of the NACA 63-415 and a Modified NACA 63-415 Airfoil*, vol. 1193, no. December. 2000.
[18] Rohmawati, I.; Arai, H.; Nakashima, T.; Mutsuda, H.; Doi, Y. "Effect of wavy leading edge on pitching rectangular wing." *Journal of Aero Aqua Bio-Mechanism*, vol. 9, no. 1, pp. 1–7, 2020.
[19] Rohmawati, I.; Arai, H.; Nakashima, T.; Mutsuda, H.; Doi, Y. "Effect of Wavy Leading Edge with Various Aspect Ratios on a Rectangular Wing" *IOP Conference Series: Earth and Environmental Science 557 – 012060*, 2020.
[20] S. Wang, D. B. Ingham, L. Ma, M. Pourkashanian, and Z. Tao, "Computers & Fluids Numerical investigations on dynamic stall of low Reynolds number flow around oscillating airfoils q," *Comput. Fluids*, vol. 39, pp. 1529–1541, 2010.
[21] A. Buchner, M. W. Lohry, L. Martinelli, J. Soria, and A. J. Smits, "Dynamic stall in vertical axis wind turbines : Comparing experiments and computations," *Jnl. Wind Eng. Ind. Aerodyn.*, vol. 146, pp. 163–171, 2015.
[22] A. Orlandi, M. Collu, S. Zanforlin, and A. Shires, "3D URANS analysis of a vertical axis wind turbine in skewed fl ows," *Jnl. Wind Eng. Ind. Aerodyn.*, vol. 147, pp. 77–84, 2015.
[23] H. R. Karbasian and K. C. Kim, "Numerical investigations on flow structure and behavior of vortices in the dynamic stall of an oscillating pitching hydrofoil," vol. 127, no. February, pp. 200–211, 2016.
[24] S. Wang, L. Ma, D. B. Ingham, M. Pourkashanian, and Z. Tao, "Turbulence Modelling of Deep Dynamic Stall at Low Reynolds Number," vol. II, 2010.
[25] K. Gharali and D. A. Johnson, "Dynamic stall simulation of a pitching airfoil under unsteady freestream velocity," *J. Fluids Struct.*, vol. 42, pp. 228–244, 2013.
[26] B. F. N. (editors) D. T. H. New, *Flow Control Through Bio-Inspired Leading Edge Tubercles*. 2020.